

AIAA 82-4022

Pointing Fluctuation of a Despun Antenna Due to Axial Thruster Firing

Tadashi Shiomi*

Radio Research Laboratories, Japan

When the axial thruster of Japan's experimental communication satellite is fired for the north-south stationkeeping maneuver, nutational motion of the satellite is induced. This degrades the pointing performance of the satellite antenna, which continues for several minutes. Analysis of satellite dynamics using a simple model predicts that the pointing fluctuation of the despun antenna, which causes a fluctuation of the communication signal levels, reaches a maximum of approximately 0.7 deg during thruster firing. This agrees with the actual measurements. By analysis, the optimum conditions for the timing and the duration of continuous firing of the canted thruster are also obtained. These depend on both spin rate and the ratio of moments of inertia of the satellite.

Introduction

JAPAN'S experimental communication satellite (CS)¹ is at 135°E longitude in a geostationary orbit, being kept within the tolerance of ± 0.1 deg in both longitude and latitude. As shown in Fig. 1 it is a spin-stabilized satellite with a mechanical despun antenna having a shaped beam² in K-band communication frequencies. The pointing accuracy required for experiments is about 0.3 deg. In order to keep this accuracy, the attitude (spin axis of the satellite) must be periodically corrected against spin-axis drift, due to the solar radiation torque, and maintained within 0.1 deg of tolerance from the orbit normal.

The attitude tolerance, however, becomes temporarily larger than 0.1 deg, due to the nutation of the spin axis when an axial thruster is fired in the continuous burn mode at a north-south stationkeeping maneuver. It consequently causes pointing accuracy degradation which continues during the maneuver. The fluctuant degradation remains even after the maneuver, though it is reduced by the nutation damper. On the other hand, a constant degradation may be induced due to spin-axis shift, which is caused by accumulated torque given by the continuous firings.

Especially in the case of a satellite, which has narrow and shaped beams like the CS, to know the characteristics of these pointing fluctuations and to find effective means of improvement are considered to be most important.

In this paper, the attitude dynamics of the CS is analyzed by using a simple axisymmetric model of the satellite. Also, the pointing fluctuation during the thruster firing is simulated, including wobble effect. Then, comparing the simulation results with the actual data of the pointing degradation measured at a ground station for the K-band beacon receiving level, it is shown that the calculation based on the simple model can well explain the measurement.

The conditions are also obtained under which, just after thruster firing, the spin-axis nutation vanishes or the spin-axis shift is not caused.

Antenna and Attitude Control System of the CS

Figure 2 shows the structure of the CS. The CS is spin stabilized with a spin rate of about 93 rpm. The despun horn-reflector antenna is driven by a brushless dc motor. The pointing control uses one of two infrared optical Earth sensors with an axis above and below the normal satellite spin

plane, which generate Earth horizon crossing reference pulses. For attitude determination, these Earth-sensor signals and one sun-sensor signal are used. The sun-sensor assembly consists of two redundant sensors, one of which, selected by ground command, produces a single pulse for each satellite revolution. The sun-sensor signals are also used as primary signals for reaction control thruster synchronization. The attitude correction maneuvers are carried out by firing one of two canted axial thrusters in the pulse firing mode. The same thruster is used for orbit plane inclination corrections (north-south stationkeeping maneuver) in the continuous firing mode. The nutation damper has a passive device consisting of a curved tube filled with neon gas and a free-rolling steel ball. The time constant of nutation damping is about 15 min.

Measurement of the Beacon Level Variation

Figure 3 shows the CS's K-band beacon level variation which was measured at the Kashima Ground Station of the Radio Research Laboratories (RRL) when a north-south stationkeeping maneuver was carried out by NASDA (National Space Development Agency of Japan) by firing one of the two canted axial thrusters of the CS. At the maneuver, in order to correct the orbital ascending node by about 180 deg, three continuous thruster firings were commanded, where each firing had a duration of 59 s and the attained ΔV was about 7.5 m/s perpendicular to the orbit plane. Figure 3 shows the beacon level variation during the first firing started at about 02:24 (Universal Time).

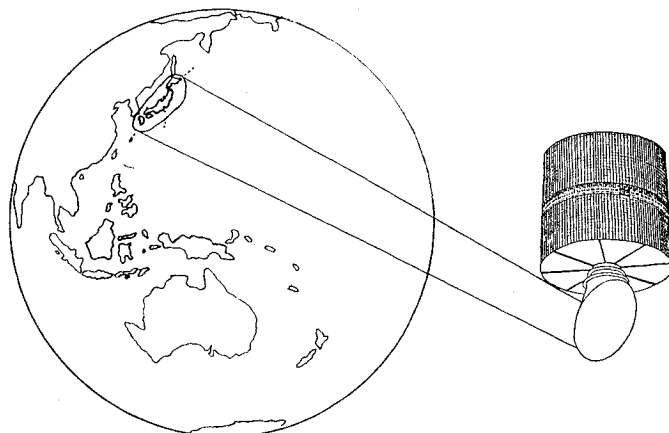


Fig. 1 The CS spacecraft and its shaped beam covering Japan's territory in K-band (30/20 GHz) frequencies.

Received July 1, 1980; revision received May 28, 1981. Copyright © American Institute of Aeronautics and Astronautics, Inc., 1981. All rights reserved.

*Technical Official, Satellite Control Section, Kashima Branch.

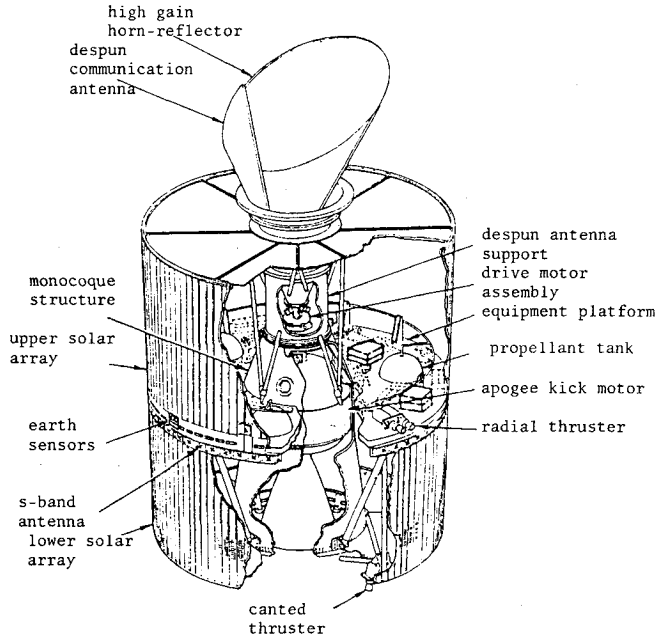


Fig. 2 CS spacecraft configuration.

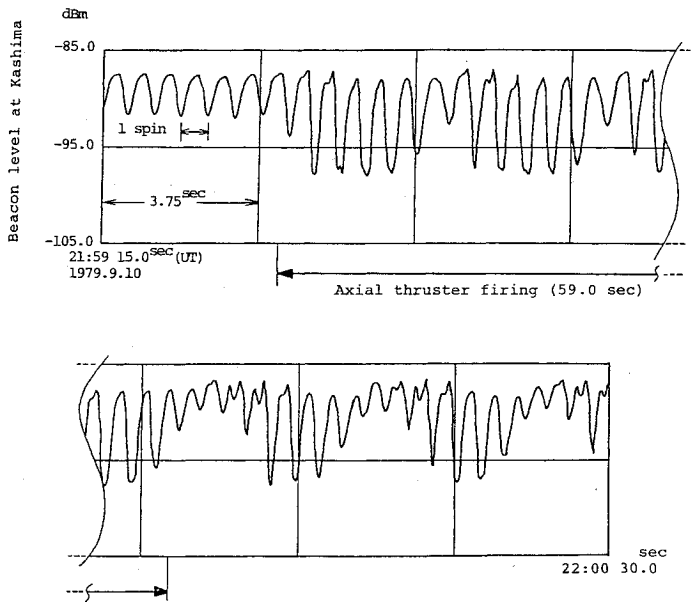


Fig. 3 Fluctuation of K-band beacon (19.45 GHz) of the CS at Kashima Ground Station during axial thruster firing.

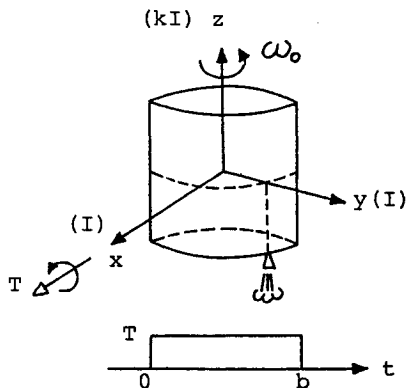
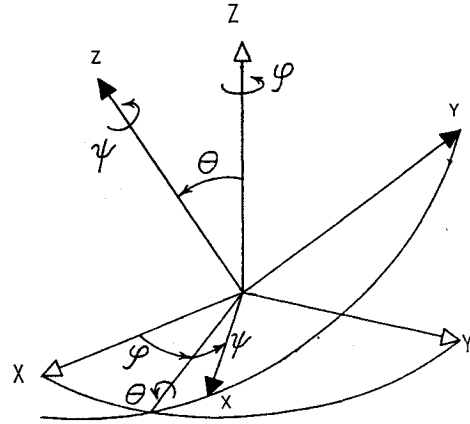
Fig. 4 Axisymmetric model of the CS where I is the moment of inertia, k is the moment of inertia ratio, and T is torque.

Fig. 5 Euler angles.

The K-band beacon level at Kashima usually has a fluctuation of about 3 dB (peak-to-peak) with the spin frequency (about 1.55 Hz) of the satellite, which are considered to be caused mainly by the satellite's wobble effect. During thruster firing, the fluctuation increases to 11 dB (peak-to-peak) periodically with a lower frequency of about 0.25 Hz. The fluctuation remains after the firing, though its amplitude decreases gradually. These variations are due to the fact that the satellite nutation, which is induced by the axial thruster firing, causes pointing fluctuation of the CS despun antenna.

It should be noted here that the receiving signal variation is not directly proportional to the pointing error, for the CS antenna is beam shaped in the K-band.

Analysis of the Spin-Axis Motion

Spin-Axis Motion Induced by Thruster Firing

Let us consider the spin-axis motion using a simple model of the satellite, since the spin-axis moment of inertia of the despun antenna horn-reflector is much smaller than that of the main body. Figure 4 shows the axisymmetric model which has an axial thruster that is fired during the period of $0 \leq t \leq b$. The torque given is assumed to have an ideal performance as shown in Fig. 4; that is, the magnitude is constant for the firing duration. The Euler equations of motion of the simplified satellite body are given as

$$\dot{\Omega}_1 + (k-1)\Omega_2\Omega_3 = T/I \quad (1)$$

$$\dot{\Omega}_2 - (k-1)\Omega_3\Omega_1 = 0 \quad (2)$$

$$\dot{\Omega}_3 = 0 \quad (3)$$

where

Ω_i = angular velocity of the body about the axis $x(i=1)$, $y(i=2)$, and $z(i=3)$

$I = I_1 = I_2$ = moment of inertia about the x or y axis

$k = I_3/I$ = moment of inertia ratio; I_3 is the moment of inertia about the z axis

T = constant thrusting torque in the x axis direction

$(\dot{})$ = time derivative

Using the definition of the Euler angles φ , θ , ψ , as shown in Fig. 5, we obtain the relations between Ω_i and the Euler angles

$$\Omega_1 = \dot{\varphi}\sin\psi + \dot{\theta}\cos\psi \quad (4)$$

$$\Omega_2 = \dot{\varphi}\cos\psi - \dot{\theta}\sin\psi \quad (5)$$

$$\Omega_3 = \dot{\varphi} + \dot{\psi} \quad (6)$$

where the spin-axis deflection angle θ is supposed to be small and the approximate relations $\sin\theta = \theta$, $\cos\theta = 1$ can be used.

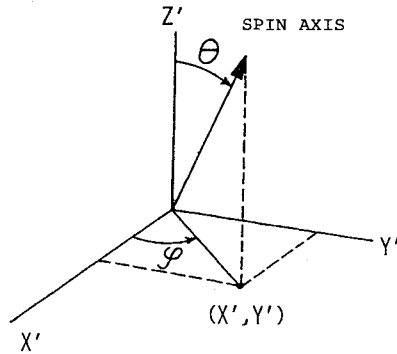


Fig. 6 Projection of the spin-axis vector on the inertial plane: $X' = \theta \cos \varphi$, $Y' = \theta \sin \varphi$ (for small θ).

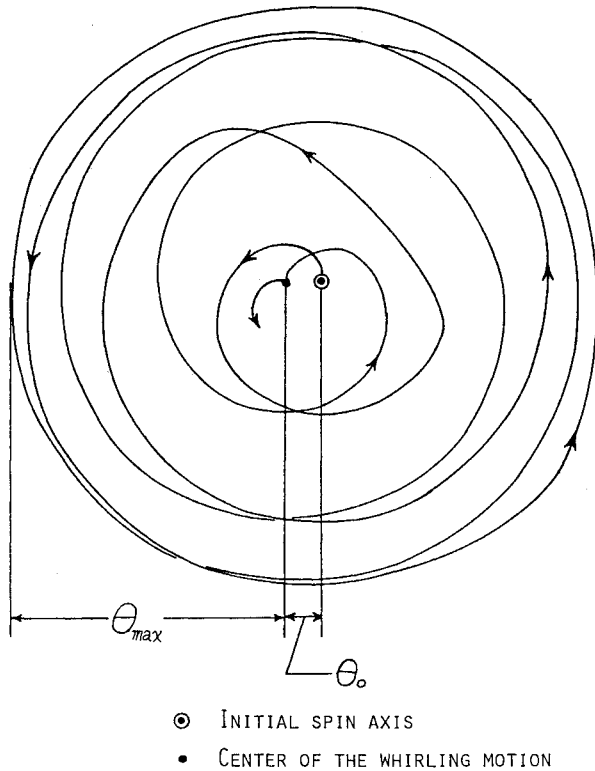


Fig. 7 Whirling motion of the spin-axis projection during the axial thruster firing, where θ_0 is the shift angle of the whirling center from the initial spin axis and θ_{\max} is the maximum whirling angle.

The solutions of the Euler equations (1-3) are substituted into the left-hand sides of Eqs. (4-6), then Eqs. (4-6) become the set of differential equations for the Euler angles. The motion of the spin axis can then be described by the projection of the unit vector along the spin axis in the plane that was perpendicular to the initial spin axis. So it is useful to solve Eqs. (4-6) for the new variables $X' = \theta \cos \varphi$ and $Y' = \theta \sin \varphi$, which are elements of the projection of the spin axis on the inertial plane (see also Fig. 6).

$$X' + iY' = \frac{T}{Ik\omega_0\omega_l} (-k + I + ke^{i\omega_0 t} - e^{ik\omega_0 t}) \quad (7)$$

($0 \leq t \leq b$ during the thruster firing)

where $\omega_l = (k-1)\omega_0$, ω_0 is the spin rate, and

$$X' + iY' = \frac{T}{Ik\omega_0\omega_l} (A + Be^{ik\omega_0 t}) \quad (8)$$

($t \geq b$ after the firing)

Table 1 Spin-axis whirling during thruster firing

Item	Magnitude	Evaluation for the CS
Shift angle of the whirling center from the initial spin axis	$\theta_0 = \frac{T}{I\omega_0\omega_l} \frac{1-k}{k}$	0.05 deg
Maximum whirling angle	$\theta_{\max} = \frac{2T}{I\omega_0\omega_l}$	0.68 deg
Coupling period	$T_c = \frac{2\pi}{(k-1)\omega_0}$	4.0 s (observation) 4.07 s

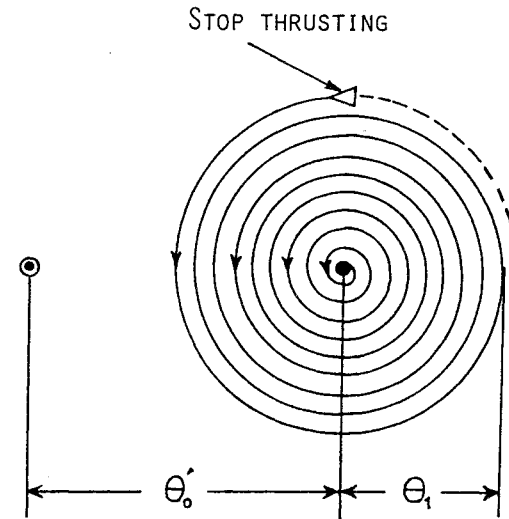


Fig. 8 Spin-axis motion after the axial thruster firing, where θ_0 is the spin-axis shift angle from the initial attitude after the convergence of the nutation and θ_l is the nutation angle just after the thruster stop.

where

$$A = (k-1)(e^{i\omega_0 b} - 1) \quad B = (e^{-i\omega_l b} - 1)$$

In the analysis, the effect of the nutation damper is not considered, but it is allowable in our case where the nutation damper has a much longer time constant than the thrusting duration.

Characteristics of the Spin-Axis Motion

Equation (7) means that during the thruster firing the spin axis has a periodic whirling motion of which the center is shifted by the angle θ_0 from the initial position of the spin axis (see Fig. 7). The maximum whirling angle θ_{\max} occurs periodically with the coupling period between the spin motion (ω_0) and the nutation ($k\omega_0$). Table 1 shows these characteristics and the evaluations for the CS, where corresponding flight data cannot be directly obtained, except the coupling period T_c which is obtained from the beacon level fluctuations as shown in Fig. 3.

Equation (8) means that after the firing, the spin-axis locus becomes a circle of which the center is related to the term A and the radius to B . The period is $2\pi/k\omega_0$; that is, the nutation period. As for the actual satellite, the nutation damper gradually reduces the nutation and the spin-axis locus converges as shown in Fig. 8. It should be noted here that the nutation magnitude θ_l and the attitude shift θ_0 depend on the thrusting duration b . Table 2 shows the conditions under which θ_l and θ_0 become maximum or minimum and the evaluations for the CS. It is desirable, of course, to make the

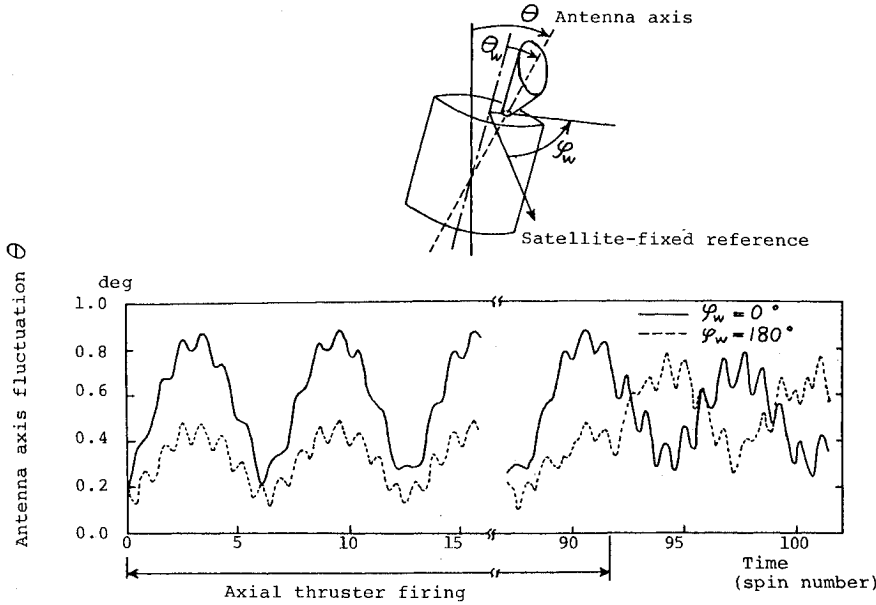


Fig. 9 Antenna pointing fluctuation due to the nutational motion during the thruster firing and the wobble, where θ is the antenna axis fluctuation angle, θ_w the wobble angle, and φ_w the wobble phase: $T = 16.62$ N-m, $I = 183.0$ kg-m², $k = 1.160$, $\omega_0 = 93.19$ rpm, $b = 59.0$ s, $\varphi_w = 0.2$ deg.

Table 2 Nutation and attitude shift after firing

Item	Magnitude	Condition ^a	Evaluation for the CS, deg
Attitude shift	$ \theta'_0 _{\max} = \frac{2T}{I\omega_0\omega_l} \frac{k-1}{k}$	$\omega_0 b = (2n+1)\pi$	0.1
	$ \theta'_0 _{\min} = 0$	$\omega_0 b = 2n\pi$	0.0
Nutation	$ \theta_l _{\max} = \frac{2T}{I\omega_0\omega_l} \frac{1}{k}$	$\omega_l b = (2m+1)\pi$	0.0
	$ \theta_l _{\min} = 0$	$\omega_l b = 2m\pi$	0.0

^a m and n are arbitrary integers.

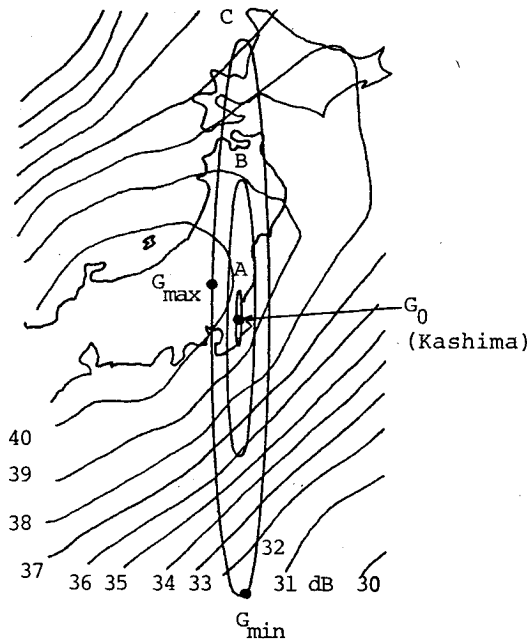


Fig. 10 Relative motion of an Earth station (Kashima) in the CS's K-band beacon antenna pattern, where the pointing fluctuation for region A is $\theta = 0.1$ deg, for B is $\theta = 0.5$ deg, and for C is $\theta = 1.0$ deg.

thrusting duration satisfy both conditions, $\omega_0 b = 2n\pi$ and $\omega_l b = 2m\pi$, when the spin-axis whirling stops without nutation just after the firing and the attitude shift does not occur.

Pointing Fluctuation of the Despun Antenna

The pointing fluctuation of the despun antenna is caused by the spin-axis motion described previously and by the wobble effect, which is the fluctuation of the despun antenna due to a small difference between the spin and the despun axis. Let us denote the wobble by the vector θ_w of which the magnitude is θ_w and the phase is φ_w , then the despun axis motion relating to the axial thruster firing can be described in the same manner as the spin-axis motion in Eqs. (7) and (8). The despun axis (X'' , Y'') is given as

$$X'' + iY'' = \frac{T}{Ik\omega_0\omega_l} (-k + 1 + ke^{i\omega_0 t} - e^{ik\omega_0 t}) + \theta_w e^{i\varphi_w t} \quad (9)$$

($0 \leq t \leq b$ during the thruster firing)

$$X'' + iY'' = \frac{T}{Ik\omega_0\omega_l} (A + Be^{(ik\omega_0 - 1/\tau)t}) + \theta_w e^{i\varphi_w t} \quad (10)$$

($t \geq b$ after the thruster firing)

where τ is the time constant of the nutation damper, and vectors A and B are the same as previously defined.

Equation (9) means that the despun axis has the similar motion as that of the spin axis, but the whirling magnitude varies depending on the wobble phase φ_w . Equation (10) means that the motion of the despun axis after the thrusting also has the whirling motion due to the coupling between the nutation term $e^{ik\omega_0 t}$ and the wobble term $\theta_w e^{i\varphi_w t}$.

Figure 9 shows numerical examples of the despun antenna fluctuations, where θ is $\sqrt{X'^2 + Y'^2}$, or the fluctuated angle of the antenna axis from the initial spin axis. The used satellite model parameters T , I , k , ω_0 , and b are those corresponding to the CS. The whirling period of about 4.0 s and the fluctuation dependence on the wobble phase φ_w are known by the figure.

In order to compare the behavior of the pointing fluctuation with the actual measured signal variation data shown in Fig. 3, we should consider the shaped-beam pattern and its relative motion to the ground station. In Fig. 10, part of the shaped-beam pattern in 19.45 GHz beacon of the CS is shown

and three elongated ellipse-like contours mean the relative motion of an Earth station at Kashima when the despun antenna has pointing errors 0.1, 0.5, and 1.0 deg and their phase varies from 0 to 2π . For example, when the pointing error is 1.0 deg, the antenna gain to the Earth station varies between ~ 40 dB (G_{\max}) and 31.5 dB (G_{\min}) depending on the pointing error phase. When the pointing error does not exist, the gain is about 39.5 dB at Kashima (G_0).

Now then, we apply the previous analytical result of the pointing fluctuation (Fig. 9) to Fig. 10 and investigate the antenna gain fluctuation which is directly related to the beacon level variation at the Kashima Ground Station. As shown in Fig. 9, pointing fluctuation magnitude θ varies between 0.2 and 0.9 deg with the period of approximately 4 s in the case of wobble phase $\varphi_w = 0$ deg. The phase variation of the pointing fluctuation— $\tan^{-1}(Y''/X'')$ in Eq. (9)—has the period of near spin, which can be shown from Eq. (9). Therefore, in Fig. 10, the relative motion of the Earth station (Kashima) is an ellipse-like whirling motion, of which the phase varies with the near-spin period and the magnitude varies with approximately 4 s between the ellipses of $\theta = 0.2$ and $\theta = 0.9$ deg. The whirling motion causes gain fluctuation for the Earth station with two major periods of spin and 4 s and the maximum amplitude of the fluctuation is found from Fig. 10 to be approximately 9 dB. This is a little smaller than the measurement. It may be due to our neglect of the despun control noise and to underestimations in our numerical evaluation shown in Fig. 9 of the wobble magnitude θ_w and thruster firing torque T . However, the whole feature and major periods of the measured level variation agree with the results of our analysis.

Consequently, the receiving level variation at the ground station shown in Fig. 3 can be explained to have been caused by a certain pointing fluctuation similar to that shown in Fig. 9 through modulation by the shaped-beam pattern motion.

Conclusions

By using a simple axisymmetric model, we analyzed the fluctuation of both the spin axis and the despun axis of Japan's communication satellite during the firing of the axial thruster for north-south stationkeeping maneuvers. The coupled pointing fluctuation among the spin motion, nutation, and wobble is not negligible, even though it causes temporary pointing degradation. By comparing the result of the analysis with the measurement, the analysis is proven to be useful to evaluate the feature and the period of the beacon level variation.

The pointing degradation is reduced to the normal level in a fraction of an hour, but the attitude may be shifted by nearly 0.1 deg under the worst condition. In such a case, it is necessary to correct the attitude so as to keep it within the allowable error.

To reduce the pointing fluctuation due to thrusting, the thruster should be set and operated so that little torque is induced at north-south maneuvers.

Acknowledgments

Thanks are due to my colleagues with whom I have discussed this problem. I also wish to thank the technical editor for valuable advice.

References

- ¹Tsakamoto, K., Otsu, Y., Kosaka, K., Shiomi, T., and Sasaoka, H., "Experimental Program and Performance of Japan's Communication Satellite (CS) and Its First Results," *IEEE Transactions on Communications*, Vol. COM-27, Oct. 1979, pp. 1392-1405.
- ²Otsu, Y., Shiomi, T., Kawaguchi, N., and Hashimoto, K., "Antenna Pattern Measurement of an In-Orbit Satellite," National Telecommunications Conference, Houston, 1980.

From the AIAA Progress in Astronautics and Aeronautics Series . . .

REMOTE SENSING OF EARTH FROM SPACE: ROLE OF "SMART SENSORS"—v. 67

Edited by Roger A. Breckenridge, NASA Langley Research Center

The technology of remote sensing of Earth from orbiting spacecraft has advanced rapidly from the time two decades ago when the first Earth satellites returned simple radio transmissions and simple photographic information to Earth receivers. The advance has been largely the result of greatly improved detection sensitivity, signal discrimination, and response time of the sensors, as well as the introduction of new and diverse sensors for different physical and chemical functions. But the systems for such remote sensing have until now remained essentially unaltered: raw signals are radioed to ground receivers where the electrical quantities are recorded, converted, zero-adjusted, computed, and tabulated by specially designed electronic apparatus and large main-frame computers. The recent emergence of efficient detector arrays, microprocessors, integrated electronics, and specialized computer circuitry has sparked a revolution in sensor system technology, the so-called smart sensor. By incorporating many or all of the processing functions within the sensor device itself, a smart sensor can, with greater versatility, extract much more useful information from the received physical signals than a simple sensor, and it can handle a much larger volume of data. Smart sensor systems are expected to find application for remote data collection not only in spacecraft but in terrestrial systems as well, in order to circumvent the cumbersome methods associated with limited on-site sensing.

505 pp., 6 × 9, illus., \$22.00 Mem., \$42.50 List

TO ORDER WRITE: Publications Dept., AIAA, 1290 Avenue of the Americas, New York, N. Y. 10019